

RSC Advances



This is an *Accepted Manuscript*, which has been through the Royal Society of Chemistry peer review process and has been accepted for publication.

Accepted Manuscripts are published online shortly after acceptance, before technical editing, formatting and proof reading. Using this free service, authors can make their results available to the community, in citable form, before we publish the edited article. This *Accepted Manuscript* will be replaced by the edited, formatted and paginated article as soon as this is available.

You can find more information about *Accepted Manuscripts* in the [Information for Authors](#).

Please note that technical editing may introduce minor changes to the text and/or graphics, which may alter content. The journal's standard [Terms & Conditions](#) and the [Ethical guidelines](#) still apply. In no event shall the Royal Society of Chemistry be held responsible for any errors or omissions in this *Accepted Manuscript* or any consequences arising from the use of any information it contains.



ARTICLE

Novel insights into L-cysteine adsorption on transition metal doped graphene: influences of the dopant and the vacancy †

Huijuan Luo,^a Hejun Li,^{*a} Zhenhai Xia,^b Yanhui Chu,^a Jiming Zheng,^c Zhengxiong Hou^d and Qiangang Fu^{*a}

Received 00th January 20xx,
Accepted 00th January 20xx

DOI: 10.1039/x0xx00000x

www.rsc.org/

Abstract: Exploring application potentials of transition metal (TM) doped graphene in biomolecular adsorption is of fundamental relevance to the area of nanobiotechnology. Herein, we investigated L-cysteine adsorption on first-row transition metal (Sc - Zn) doped single-vacancy and double-vacancy graphenes (MSVs and MDVs) using density functional theory calculations. Three kinds of upright adsorption configurations, via unprotonated S-end, O-end and N-end functional groups were considered. All MSVs chemically adsorb L-cysteine with no regular variation tendency. MDVs show decreasing chemisorption from V to Co, followed by emergence of physisorption from Ni to Zn. L-cysteine adsorption on MDVs is weaker than on MSVs, starting from Mn to Zn. Both the TM dopant and the vacancy type contribute to adsorption tendency. Besides, site-specific chemisorption is revealed. Adsorption magnetic behaviour is also interesting. In particular, FeSV, ZnSV and NiSV become magnetic after O-end, N-end and all three end-type adductions, respectively. L-cysteine adsorption induced distribution of the increasing 3d electron and TM-C interactions could account for magnetism mechanism. Interesting magnetization patterns of MSVs and MDVs occur in most magnetic chemisorbed systems, exhibiting different mirror symmetry. This study could facilitate applications of TM doped graphenes in biosensing, biomolecules immobilization, magnetic bioseparation and other fields in bionanotechnology.

1. Introduction

There is growing attention in developing nanobiotechnology, one necessary aspect of which is to find and utilize nanomaterials that are able to mediate the related processes, including adsorption of biomolecules in appropriate positions, structures and orientations on specific scaffolds of interest.

Graphene materials possess fascinating physical and chemical properties as well as facile modifications of the flexible structure. In the last decades, more and more research efforts have been made to extend application potentials of graphene in nanobiotechnology. Biosensing [1, 2], drug/gene delivery [3-5], biocatalysis [6, 7] and antibacterial materials [8, 9] are only a few out of many potential applications that are brought forward by exploiting the two-dimensional, monolayer, sp²-bonded carbon network. Biomolecules attachment on graphenes, in appropriate positions, structures and orientations, plays fundamental roles in synergistic interactions between

biomolecules and graphenes. These interactions are of vital importance in various bioapplications, including adjusting detection sensitivity and stability of biosensors, facilitating biomolecules assembly with selectivity and affinity, tuning catalysis activity, and achieving anti-bacteria function etc.. Current theoretical and experimental studies mainly focus on adsorption of biomolecules on pristine graphene [9-14], graphene oxides [8, 15-18], non-metal (mainly B [19, 20], N [19-21], S [22, 23]) doped graphenes and metal nanoparticles decorated graphenes [24-27], with the development of experimental availability of these graphene materials [28-32].

Recently, several works on fabrication of transition metal (TM) embedded graphene materials with single-atom precision, by using electron beam irradiation and subsequent magnetic sputtering or evaporation of respective metals, have been reported [33, 34]. Owing to the high capability of *in-situ* observation and the high capability of tunable processing conditions, TM embedded graphenes with different numbers of vacancies have been fabricated and observed. As uncovered experimentally [33, 34] and theoretically [35-39], both the metal dopant and the vacancy show significant modulation on geometrical, electronic and magnetic features of TM embedded graphenes. On the other hand, it has been demonstrated that doping TM atoms into graphene could effectively tune the molecular adsorption [40-43] and molecular catalysis [44]. With respect to the interactions between biomolecules and TM doped graphene, related research [45] is very rare. Therefore, intensive work to explore TM doping effects on the interactions

^a State Key Laboratory of Solidification Processing, Carbon/Carbon Composites Research Centre, Northwestern Polytechnical University, Xi'an 710072, People's Republic of China

^b Department of Chemistry, University of North Texas, Denton, TX 76203, USA

^c National Key Laboratory of Photoelectronic Technology and Functional Materials (Cultural Base), Institute of Photonics and Photo-technology, Northwest University, Xi'an 710069, PR China

^d High Performance Computing Centre, Northwestern Polytechnical University, Xi'an 710072, People's Republic of China

† Electronic Supplementary Information (ESI) is available. See DOI: 10.1039/x0xx00000x

RSC Advances

between graphene and biomolecules is of critical relevance and highly desirable. To achieve this, we selected a series of first-row TM atoms (from Sc to Zn) doped single-vacancy and double-vacancy graphenes for investigation of biomolecular adsorption. To assure consistent comparability with our previous study [45], L-cysteine was still chosen as the probe biomolecule.

In this work, the adsorption of L-cysteine (l-cys) on the single-vacancy and the double-vacancy graphenes doped with the first-row transition metals, namely Sc, Ti, V, Cr, Mn, Fe, Co, Ni, Cu and Zn, was investigated by using density functional theory (DFT) calculations. The main objective is to unveil the effects of the type of the transition metal and the type of the vacancy on adsorption behavior and magnetism of the l-cys/graphene materials. Proper explanations for adsorption stability and magnetism have also been proposed. Our results could provide a useful reference for TM-doped graphenes application in biological fields.

2. Modelling and calculation details

2.1 Models building

In the present calculations, transition metal (TM=Sc-Zn) embedded graphenes were built on the model of the optimized 6×6 intrinsic graphene sheet, with the lattice parameters being 14.76, 14.76 and 20.00 Å in the a, b and c directions, respectively. Replacing the C atom by a transition metal atom at the centre of the intrinsic graphene supercell, the corresponding TM embedded single-vacancy graphene (MSV, M=Sc-Zn) was obtained. Replacing two C atoms by a transition metal atom at the centre of the intrinsic graphene supercell, the corresponding TM embedded double-vacancy graphene (MDV, M=Sc-Zn) was obtained. The doping concentrations are 1.38% and 1.41% for MSV and MDV, respectively. In addition, the MG (M=Sc-Zn) term is introduced, for simplicity, to denote corresponding MSV and MDV with the same TM dopant.

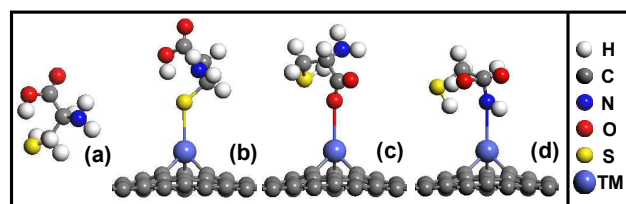


Fig. 1 Structure illustration of L-cysteine (a), unprotonated S-end (b), O-end (c) and N-end (d) l-cys adsorption on MGs before DFT calculations.

With respect to the docking geometry of a single l-cys on MGs, three kinds of upright adsorption configurations (Fig. 1), ie, through the unprotonated S-end, O-end or N-end functional group, were considered. The S, O or N atom in l-cys was initially located directly on top of the dopant in MG (M=Sc-Zn) at the distance of 3 Å. The upright adsorption configurations of l-cys, with one head group attached to graphene and the other two extending away towards the vacuum, are of intense

significance. Upright l-cys could act as an anchoring site, either polymerizing through the free amino or carboxyl groups or incorporating metal ions through any free functional groups of the three [46, 47]. For convenience, the S-end, O-end and N-end l-cys/graphene adducts were labelled as S-MSV, O-MSV, N-MSV and S-MDV, O-MDV, N-MDV for MSV and MDV, respectively. Optimized adsorption configurations were obtained through full relaxation.

2.2 Calculation parameters

Dispersion-corrected density functional theory (DFT-D) calculations were carried out by using the DMol³ package in Materials Studio [48]. The Perdew-Burke-Ernzerhof (PBE) exchange-correlation functional of the GGA-type was employed, with long-range dispersion correction via the Grimme's scheme [49]. The DFT-D approach was applicable to the present systems, as validated in our previous work [45]. The double numerical basis set augmented with polarization function (DNP) was chosen as the basis set. The DFT semicore pseudopotentials (DSPP) core treatment was applied.

Structural optimization was carried out on all systems without any constraint, with convergence tolerances of 1.0×10^{-5} Hartree on energy, 1.0×10^{-3} Hartree on gradient and 1.0×10^{-5} on displacement. The SCF convergence criterion of 1.0×10^{-6} Hartree on energy was achieved with respect to the $6 \times 6 \times 1$ k-point sampling over the Brillouin zone. Magnetic moments were computed using the Mulliken analysis method. The isolated l-cys molecule, the MG sheet and the l-cys/MG adsystems were calculated, without any constraint, under the same parameters to ensure the comparability of the results.

2.3 Binding energy

The binding energy, E_b , of the substitutional transition metal atom in the single-vacancy or double-vacancy graphene was calculated [35] as

$$E_b = E_{MSV} - E_{TM} - E_{SV} \quad (1)$$

$$E_b = E_{MDV} - E_{TM} - E_{DV} \quad (2)$$

where E_{MSV} and E_{MDV} denoting the total energy of the optimized MSV and MDV, E_{TM} the total energy of an isolated TM atom, E_{SV} and E_{DV} the total energy of the reconstructed single-vacancy and double-vacancy graphene, respectively.

To evaluate the adsorption stability of l-cys on MG systems, the binding energy E_b was calculated [50, 51] as

$$E_b = E_{tot} + 1/2E_{H_2} - E_{MG} - E_{l-cys} \quad (3)$$

where E_{tot} denoting the total energy of the optimized l-cys/MG adduct, E_{MG} the total energy of MG, including MSV and MDV, E_{l-cys} the total energy of a l-cys molecule, and E_{H_2} the total energy of a hydrogen molecule, respectively. Unprotonated cysteine is not the most stable species in the gas phase. We assume that the hydrogen atoms dissociated from the cysteine form molecules. For that reason, we consider the total energy E_{H_2} of the gas-phase H_2 molecule [50, 51]. The more negative value of E_b means a more stable structure and a stronger binding energy.

3. Results and discussion

In the following sections, geometrical optimizations of MSVs and MDVs (M=Sc-Zn) were first performed, providing initial structures and magnetic characteristics for subsequent investigation on l-cys adsorption. Then adsorption stability of l-cys on MSVs and MDVs was evaluated by discussing E_b values, charge density distributions and geometrical structures. Adsorption mechanism was proposed. Finally, magnetism of the l-cys/MG adducts was presented, by analyses of spin density distribution and Mulliken spin population, followed by analyses of magnetism mechanism. Magnetization symmetry was also exhibited.

3.1 The main properties of MGs

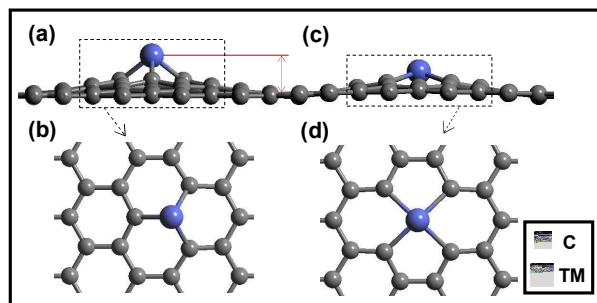


Fig. 2 Typical atomic configurations of relaxed MSV: side view (a), top view (b) and MDV: side view (c), top view (d). h denotes elevation of the TM dopant, relative to average height of carbon atoms.

Typical optimized configurations of MSVs and MDVs are shown in Fig. 2. The binding energies of the MSV series (Fig. 3(a)) for TM doping are in the range of $-12 \sim -2$ eV. The change behaviour is non-monotonic. Ti [$3d^24s^2$] presents a local stronger binding energy, with the four valence electrons saturated [35]. Local weaker binding energies among the 3d transition metals are found for Cr and Mn. For Cu and Zn, with almost full d-shells, much weaker binding energies are observed. The E_b values of the MDV series show a similar non-monotonic trend from Sc to Zn. These non-monotonic behaviours are related to the simultaneous energy down-shift and compression of the 3d shell of the metal as we increase the atomic number [39].

With respect to specific geometrical changes, the TM atom of MSVs is displaced outwards from the graphene surface owing to a larger atomic radius relative to carbon (Fig. 2(a)). The elevation trend of the dopant is shown in Fig. 3(b). Neighbouring carbon atoms are also protruded outwards to facilitate the formation of three transition metal-carbon (TM-C) bonds. The average TM-C bond lengths (Fig. 3(c)) are all below the sum of the covalent radii [52] of TM (from Sc to Zn) and C, in consistence with strong chemical binding. Besides, the average TM-C bond length decreases from Sc to Fe as the atomic size increases, and then it goes up as the bonding becomes weaker. In most cases, the transition metal atom forms three equivalent TM-C bonds with neighbouring carbon atoms (Fig. 2(b)) for TM=Sc-Ni. CuSV and ZnSV suffer Jahn-Teller-

like distortion, with the lengths of the three Cu-C bonds and the three Zn-C bonds are 1.87, 1.89, 1.87 Å and 1.89, 2.02, 1.89 Å, respectively. The behaviour of MDVs is kind of simplicity. All MDVs form the “cross” configuration (Fig. 2(d)), with the TM dopant equally bonded to neighbouring four carbon atoms. Due to combined interactions of atomic size and bonding strength, the TM dopant is also elevated and the covalent TM-C bond length is also changed (Fig. 3 (b, c)). For CuG and ZnG, the introduction of bigger vacancies leads to stronger binding ability, due to the Jahn-Teller-like effect in the single-vacancy case.

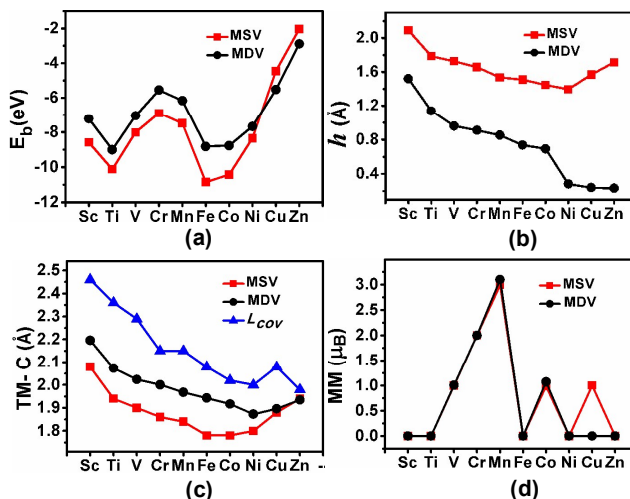


Fig. 3 (a) The binding energy E_b , (b) elevation h of the TM dopant, (c) average TM-C bond length and (d) magnetic moment (MM) of MSVs and MDVs. L_{COV} in (c) indicates the sum of the covalent radii of TM and C.

The magnetic properties are presented in Fig. 3(d) and Tab. S1. The MGs (M=V, Cr, Mn) and CoDV are magnetic with dominant 3d magnetism. MSVs (M=Co, Cu) are magnetic with large contribution of carbon atoms in graphene. These calculated results of MSVs are in good accordance with previous findings [35, 39]. Mild discrepancies in the MDV systems appear under our calculation scheme. FeDV shows no magnetism, which is different from the magnetic moments of $\sim 3.2 \mu_B$ in Ref [35].

3.2 Adsorption stability of the l-cys/MG adducts

3.2.1 Adsorption stability of the l-cys/MSV adducts

The binding energies of the l-cys/MSV adducts (Fig. 4) are all below -0.75 eV, suggesting all kinds of unprotonated l-cys are chemically adsorbed on the MSV substrate. No general variation trend appears in the values of E_b along with the TM series from Sc to Zn. Fig. S1 of ESI† shows the typical charge density graphs. Large overlap in charge density is observed, indicating existence of stable adsorptions. Comparison of the E_b values of the l-cys/MSV adducts reveals that different kinds of MSVs exhibit distinct adsorption affinities towards each functional group (Fig. S1, ESI†). Cr-Co and Zn doped single-vacancy graphenes show the best affinity towards the S-end l-

cys radical, while Sc, Ti, V, Ni and Cu doped single-vacancy graphenes show the best adsorption stability towards the O-end radical. The N-end adduction is always the weakest adsorption type for all systems.

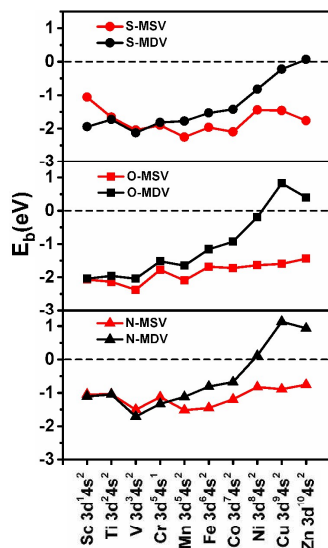


Fig. 4 E_b of l-cys/MSVs and l-cys/MDVs with different end-types of l-cys adsorbed.

The MSV substrates endure strain relaxation to contribute to the strong binding (Fig. 5(a-d)). On one hand, the positions of the TM dopant (Fig. 6(a)) and neighbouring carbon atoms change obviously. The lengths of the average TM-C bonds vary (Fig. 6(b)) for different types of transition metals. Concerning ZnSV, the average length of the Zn-C bond (2.28 - 2.30 Å) is surprisingly much higher than the sum of the covalent radii (1.98 Å). Further investigation on geometrical structures reveals intensified Jahn-Teller distortion. Two Zn-C bonds are broken, and only one Zn-C binding remains to adsorb l-cys (Fig. 5(d)). Meanwhile, the Zn dopant is largely elevated out. In contrast, most of the bond lengths and bond angles of l-cys are not obviously changed after adsorption, except for the angles related to adsorbed functional groups, which are greatly changed.

For all l-cys/MSV adducts through the S-end chemisorption, the covalent TM-S bond forms (Fig. 5(a)), with the -COOH and -NH₂ groups free extending outwards. The bonding distance between l-cys and the graphene substrate (G-L) monotonously decreases from ScSV to CoSV, then goes up to ZnSV (Fig. 7(a)). For O-end adsorption, two-site adsorption modes (Fig. 5(b)) exist for all kinds of MSVs (Tab. S2). The -COOH group becomes very close to the graphene surface, with the C-O bond shortened to 1.28 Å and the C-O= bond lengthened to 1.28 Å. Both O atoms bind the metal dopant. The two TM-O bonds are almost equal in length, and the average value varies in the range of 2.00-2.20 Å along with the change of the type of the TM dopant (Fig. 7(b)). A large steric hindrance, arising from the two TM-O bonds, exists to keep the upright adsorption configuration robust. It is noted that starting from CrSV, the average bond length is larger than the sum of the covalent radii

of the corresponding linking atoms, which is due to the combined effects of the bi-O (denoting two-site O-end adsorption) adsorption mode and the decreasing adsorption ability. Regarding N-end adduction, one-site adsorption through the formation of M-N covalent bond exists for most MSVs, with the -COOH and -SH free extending outwards (Fig. 5(c)). The bonding distance between l-cys and the graphene substrate monotonously decreases from ScSV to CuSV basically, with the exception of Fe (Fig. 7(c)).

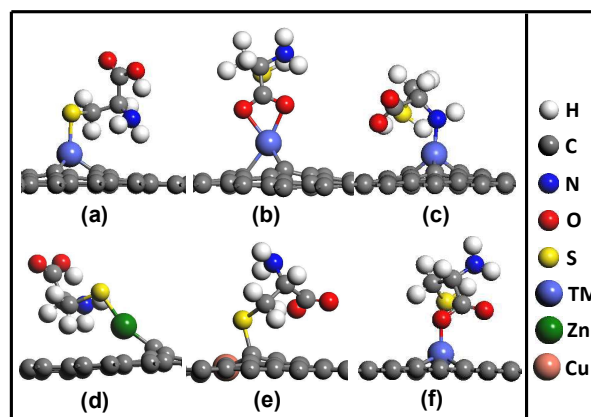


Fig. 5 Typical adsorption geometries of l-cys on MGs to illustrate S-end adsorption with a single TM-S bond (a), O-end adsorption with two TM-O bonds (TM-OH and TM-O=) (b), N-end adsorption with a single TM-N bond (c), special adsorption structures of the S-ZnSV (d), S-CuDV (e) adducts, and O-end adsorption with a single TM-O bond (O in -OH) (f) on MDV.

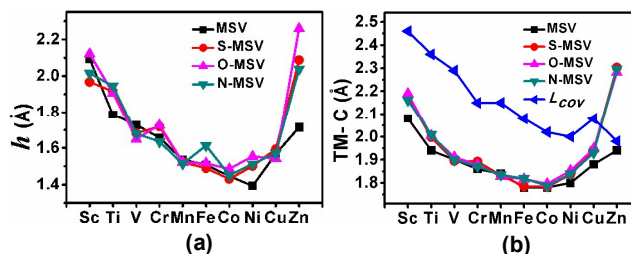


Fig. 6 (a) The elevation h of the TM dopant and (b) the average TM-C bond length in MSVs. L_{cov} indicates the sum of the covalent radii of TM and C.

3.2.2 Adsorption stability of the l-cys/MDV adducts

With respect to l-cys docking on MDVs, the E_b values (Fig. 4) uncover interesting transition from negative to positive along the TM series from Sc to Zn. For l-cys docking on MDV (M=Sc-Co), all related E_b values are less than zero, showing strong chemisorption towards the three kinds of l-cys radicals. Nevertheless, NiDV shows strong chemisorption towards the S-end l-cys (-0.82 eV), weaker chemisorption towards the O-end l-cys (-0.20 eV) and physisorption towards the N-end l-cys (0.12 eV). Regarding CuDV, only the S-end immobilization is chemically stable (-0.22 eV), while the other two kinds of l-cys radicals are physisorbed, with positive values of E_b . ZnDV

shows physical adsorption towards all the three kinds of l-cys radicals.

The weakest binding energies (~ 1 eV) for O-end and N-end adsorption among the metals studied here appear for Cu with filled d electronic shells and half-filled s electronic shells. However, for Zn, with filled d electronic shells and filled s electronic shells, O-end and N-end physisorptions are stronger than Cu. The observation may be ascribed to distinct activity of Cu relative to Zn under specific configurations. With respect to S-CuDV, one of the four carbon atoms around the Cu dopant is protruding out and a S-C covalent bond (1.87 Å) is formed (Fig. 5(e)). The finding of S-C bond in S-CuDV also suggests neighbouring carbon atoms should be active [53] in molecular adsorption. More investigation on chemical activity of neighbouring carbon atoms around the TM dopant is being undertaken.

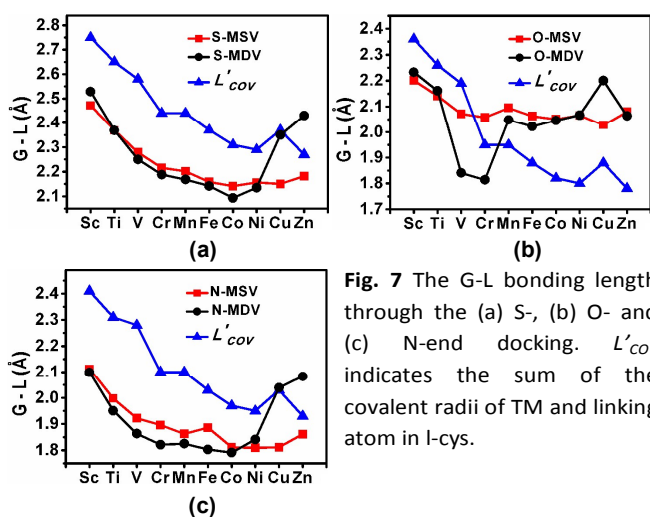


Fig. 7 The G-L bonding length through the (a) S-, (b) O- and (c) N-end docking. L'_{cov} indicates the sum of the covalent radii of TM and linking atom in l-cys.

In the case of adsorption on MDVs ($M=Sc-Cu$), charge density distributions (Fig. S2, ESI†) are similar compared to the MSVs cases. Much overlap appears for all adsorption configurations, showing stable adsorption for both chemisorption and physisorption. Compared to our results in Ref [45], no overlap exists for inert adsorption of l-cys on pristine graphene, thus the overlap here indicates more reactivity for TM doped double-vacancy graphenes. This also suggests sensing potential of NiDV, CuDV and ZnDV, taking advantage of the relatively stable physisorption. Meanwhile, the interesting findings would provide a meaningful theoretical reference in practical applications about selecting appropriate dopants for physisorption or chemisorption towards adsorbates.

Geometrical distortions are more gentle compared to the MSVs cases. The graphene substrate undergoes mild geometrical distortions. Metals are elevated and neighbouring carbon atoms are mildly protruded out by the l-cys (Fig. 8). Structural changes in l-cys are not obvious.

For the S-end adduction, most adsystems show one-site adsorption, with the single TM-S binding (Fig. 5(a)), while two-site adsorption occurs on ScDV with one Sc-O= bond formation in addition to the Sc-S bond (Fig. S3, ESI†). The

TM-S binding distance is shorter than that of the corresponding MSV cases from TiDV to NiDV, while larger for ScDV, CuDV and ZnDV (Fig. 7(a)).

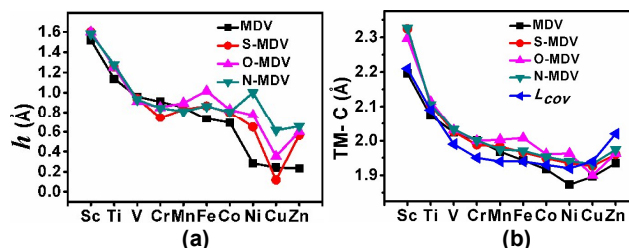


Fig. 8 (a) The elevation h of the TM dopant and (b) the average TM-C bond length in MDVs. L_{cov} indicates the sum of the covalent radii of TM and C.

For the O-end adduction, the bi-O adsorption mode (Fig. 5(b)) is favoured by the Sc, Ti, Mn, Fe, Co, Ni doped double-vacancy graphenes, while VDV and CrDV exhibit mono-O (binding through O in OH) adsorption (Fig. 5(f)). Owing to the single site burdening the whole chemisorption, the formed TM-O bond is quite shorter than that under the bi-O mode (Fig. 7(b)), compared to other kinds of MDVs. The physisorbed systems of CuDV and ZnDV also exhibit mono-O adsorption, with the Cu-O and Zn-O bonds greatly larger than the sum of the covalent radii. The TM-O binding distance is shorter than that of the corresponding MSV cases from ScDV to CrDV, while larger from MnDV to ZnDV (Fig. 7(b)).

With respect to the N-end adduction, all adsystems show one-site adsorption with the mere TM-N binding (Fig. 5(c)). N-NiDV, which is on the border between chemisorption and physisorption, has an E_b value of 0.12 eV. The N-Ni bond is 1.84 Å, a little larger than the theoretical covalent bond, in consistence with weak adsorption. The TM-N binding distance is shorter than that of the corresponding MSV cases from ScDV to CoDV, while larger from NiDV to ZnDV (Fig. 7(c)).

3.2.3 Site-specific adsorption phenomena

Herein, site-specific chemisorption (Tab. 1) appears by analyses of the most stable adsorption configurations. Under the situation of single-vacancy graphenes, the S-end l-cys docking on Cr-Co and Zn doped graphenes is stronger than the -COOH or -NH₂ docking, whereas the O-end l-cys shows the best stability on Sc, Ti, V, Ni and Cu doped single-vacancy graphenes. Under the situation of double-vacancy graphenes, the S-end l-cys docking on V-Zn doped graphenes is stronger than the -COOH or -NH₂ docking, whereas the O-end l-cys shows the best stability on Sc and Ti doped double-vacancy graphenes. That is to say, for CrG-CoG and ZnG, S-end immobilization shows the most affinity regardless of the vacancy type; for ScG and TiG, O-end immobilization shows the most affinity regardless of the vacancy type; and VG, NiG, CuG's adsorption affinity is easily affected by the vacancy. Moreover, the capability of docking the N-end l-cys to the graphene surface is weakest in all l-cys/graphene systems. It is consistent with the fact that exploiting the amino group to bind l-cys to the metal surface is plausibly hindered in most cases

where l-cys is the anchoring group of proteins to surfaces, because the NH₂ fragment is engaged in peptide bonds along the primary chain. [51]

Tab. 1 The most stable adsorption on MSVs and MDVs.

| | Sc | Ti | V | Cr | Mn | Fe | Co | Ni | Cu | Zn |
|-----|----|----|---|----|----|----|----|----|----|----|
| MSV | O | O | O | S | S | S | S | O | O | S |
| MDV | O | O | S | S | S | S | S | S | S | S |

Therefore, site-specific chemisorptions, including site-type-specific and site-number-specific chemisorptions, could be realized through tuning the kind of the metal dopant and the kind of the vacancy in the graphene substrate. The interesting findings could provide references for nanobiomedicine fields, nanocrystal growth, decoration of graphenes and biocatalysis etc..

3.2.4 Adsorption mechanism analyses

The adsorption mechanism could be understood from the following aspects: (i) the TM dopants, which possess different numbers of outer-shell 3d electrons, and show different hybridization preferences; (ii) the vacancy types, which contribute different TM-C interactions, including different hybridization environments and different bond lengths between TM atoms and neighbouring carbon atoms.

The role of the TM dopant could be firstly deduced from l-cys adsorptions on MDVs, which show a decreasing tendency from V to Zn. The starting minima of VDV result from saturated bonds formation using all the five valence electrons of V (3d³4s²). Along with the increase of the number of 3d electrons starting from V, redundancy in electrons appears. The 3d shell becomes gradually occupied and moves to lower energies. The hybridization near the Fermi energy (E_F) is reduced (Fig. S4, ESI†). In the meanwhile, nearly few changes happen in the space nearby. This causes increase in electron repulsion, and thus causes decrease in binding interactions, even the occurrence of physisorptions.

Another role of the TM dopant is to influence TM-C interactions, illustrated together with the role of vacancy types. The TM-C interactions involve the TM-C bonding distance and the TM's preferences to hybridization environments. For TM=Sc-Cr, although shorter TM-C bonding distances occur in the case of MSVs than MDVs (Fig. S5, ESI†), different preferences to the SV or DV coordination environment lead to no obvious variation tendency of E_b values. Thus for TM=Sc-Cr, the contribution of TM's preferences to hybridization environments is larger than interactions represented by the bonding distance. For TM=Mn-Ni, l-cys chemisorption on MDVs is generally weaker, accompanied with longer TM-C bonding distances (Fig. S5), compared to corresponding chemisorption on MSVs. This also means weaker roles of coordination environments preferences compared to the role of the bonding distance, relative to TM=Sc-Cr. For TM=Cu-Zn, coordination environments play a key role, since the average TM-C bonding distance (Fig. S5) of MSVs are comparable (for

Cu) to or much larger (for Zn) than that of MDVs. Meanwhile, in the case of the single-vacancy environment, chemisorptions occur with intensified Jahn-Teller distortion in hybridization environment, even including two Zn-C bonds broken. In the case of the double-vacancy environment, the metals remain affording four TM-C bonds and show physisorptions towards l-cys.

It is noted that adsorption on MDVs shows a regular variation tendency from VDV, while adsorption on MSVs shows no regular variation tendency from VSV. This is attributed to different TM-C interactions. In MSVs, strong TM-C interactions, contributed by the short TM-C bonding length coupled with hybridization preferences, outperform the role of TM's outer-shell 3d electron redundancy. The complicated TM-C interactions lead to no regular variation trend in the E_b values along with the TM series from Sc to Zn.

3.3 Magnetism analyses

3.3.1 Magnetic properties of l-cys/MSV adducts

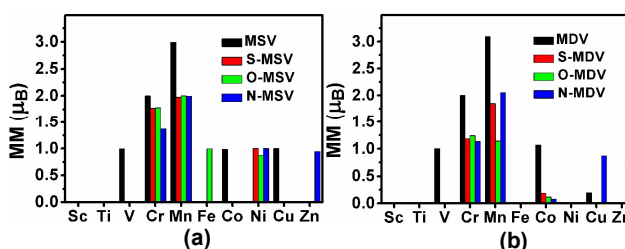


Fig. 9 The magnetic moment (MM) of the (a) MSV and l-cys/MSV adsystems and (b) MDV and l-cys/MDV adsystems.

The magnetic moments of the l-cys/MSV adsystems, along the TM series from Sc to Zn, are presented in Fig. 9. For Sc and Ti, no change in magnetism appears for the l-cys/ScSV and l-cys/TiSV adducts after any of the three kinds of end-group adsorption. The original spin polarization of l-cys radicals are quenched to zero, which is attributed to loss of unpaired electrons under strong chemical interactions.

VSV, CrSV and MnSV, in which the magnetic moments dominantly come from 3d orbitals spin polarization, l-cys adsorption induced magnetic variation is illustrated as follows. The disappearance of magnetism of VSV happens after l-cys immobilization regardless of the docking site. The initial spin moment of 2.00 μ_B of CrSV is reduced to 1.77 μ_B , 1.78 μ_B and 1.37 μ_B , respectively, for the S, O, N-end adduction. The spin density distribution (O-CrSV as an example in Fig. 10(a)) shows that most of the magnetization still locates on the TM dopant, arising from 3d orbitals spin polarization. The carbon atoms present ferromagnetic coupling within separate sublattices and antiferromagnetic coupling between sublattices, suggesting sublattice symmetry breaking. More reduction occurs in the MnSV systems. The magnetic moments reduce from 2.99 μ_B to 1.98 μ_B , 2.00 μ_B and 2.00 μ_B , respectively. Both 3d magnetism of Mn and 2p_z spin polarization of the neighbouring carbon atoms contribute to the magnetization. The linking atoms S, N, O in O= or OH also show kind of mild magnetism.

Interesting changes happen in the l-cys/FeSV adsystems. For FeSV, the S-FeSV and N-FeSV adducts remain non-magnetic, while the O-FeSV adduct becomes magnetized, with a magnetic moment of $1.00 \mu_B$ per unit cell. The magnetic moment mainly locates on Fe ($1.11 \mu_B$), indicating awakening of the 3d magnetism (Fig. 10(b)) of Fe by the O-end adsorption. The spin moments of O atoms in O= and OH are $-0.01 \mu_B$ and $-0.01 \mu_B$, respectively. The other atoms in l-cys exhibit no spin moment.

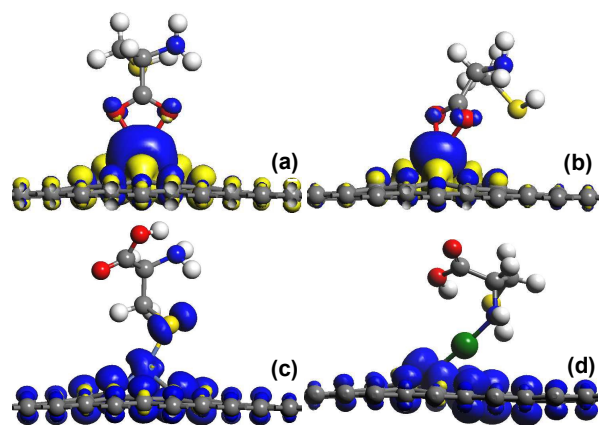


Fig. 10 Schematic side views of spin density distribution of O-CrSV (a), O-FeSV (b), S-NiSV (c) and N-ZnSV (d). The isovalue is $0.01 e \text{ \AA}^3$. The dark blue and light yellow surfaces correspond to majority and minority spins, respectively.

We put the analyses of the late transition metals Co, Ni, Cu and Zn doped single-vacancy graphenes together, since the magnetic moment oscillates between 0 and $1.00 \mu_B$. After l-cys adsorption, CoSV shows completely quenching off in magnetism from $1.00 \mu_B$ to $0 \mu_B$. In the l-cys/NiSV adsystems, completely switching on of magnetism up to $1.00 \mu_B$, $0.88 \mu_B$ and $1.00 \mu_B$ per unit cell exists (Fig. 10(c)), with $0.11 \mu_B$, $0.03 \mu_B$ and $0.13 \mu_B$ coming from Ni. The linking atoms S, O, N are $0.07 \mu_B$, $0.00 \mu_B$, and $0.01 \mu_B$, respectively, while other atoms in l-cys contribute no spin polarization. In the CuSV adsystems, l-cys immobilization quenches the magnetism to zero for all three kinds of adsorption. For ZnSV, N-end adsorption induces switching on of the magnetism up to $0.95 \mu_B$ (Zn: $0.01 \mu_B$) per unit cell (Fig. 10(d)), while the S- and O-end adsorptions lead to no influence on magnetism. For the above magnetic adsystems, the spin moment mainly comes from graphenic carbon atoms owing to spin polarization of $2p_z$ orbitals, vividly depicted by the spin density distribution graphs in Fig. 10(c, d). The linking atoms S, O in O= or O in OH and N also exhibit kind of magnetism.

3.3.2 Magnetic properties of l-cys/MDV adducts

With respect to l-cys docking on MDVs, interesting transition from chemisorption to physisorption happens along with the TM series from Sc to Zn. Therefore, we first discuss the cases of MDVs ($M = \text{Sc-Co}$), which show chemisorption towards all the three kinds of l-cys radicals. ScDV and TiDV remains non-

magnetic whether l-cys is adsorbed or not. The magnetic VDV system changes into non-magnetic after l-cys docking, regardless of the end type. Reduction in magnetism happens after l-cys docking on CrDV and MnDV, with most of the spin moment still populates on Cr and Mn (Fig. 11(a)), respectively. FeDV remains non-magnetic for all three kinds of adsorption. Regarding magnetic CoDV, possessing a magnetic moment of $1.00 \mu_B$, the magnetic moment decreases drastically and nearly diminishes, showing $0.19 \mu_B$, $0.12 \mu_B$ and $0.08 \mu_B$, respectively, for the S-end, O-end and N-end dockings. The magnetic moment mainly comes from negligible 3d spin polarization of Co (Fig. 11(b)).

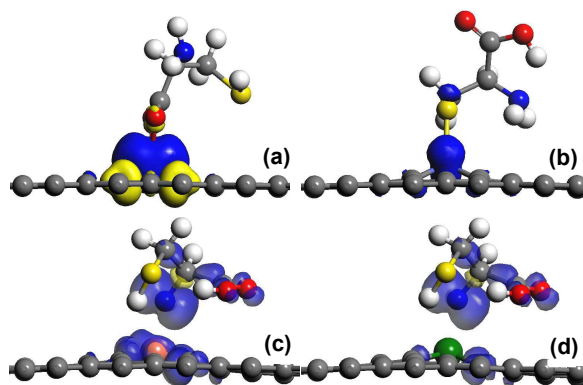


Fig. 11 Schematic side views of spin density distribution of the O-MnDV (a), S-CoDV (b), N-CuDV (c) and N-ZnDV (d) adducts. The isovalue is $0.01 e \text{ \AA}^3$. The dark blue and light yellow surfaces correspond to majority and minority spins, respectively.

Then we go to magnetic properties of the l-cys/MDV ($M = \text{Ni, Cu, Zn}$) adsystems. Regarding NiDV, the S-end and O-end chemical adductions couldn't change the non-magnetic feature. The magnetic moments of the l-cys radicals are quenched to zero due to loss of unpaired electrons induced by chemisorption. For the N-end adduction, although it shows physical adsorption, the system is still non-magnetic, with disappearance of spin polarization of l-cys. Concerning CuDV, the S-end and O-end chemical adductions induce no magnetism. The N-end physical adduction retains the magnetism of l-cys radicals (Fig. 11(c)), with a magnetic moment of $0.87 \mu_B$ per unit cell. With respect to the non-magnetic ZnDV, the N-end adduction (Fig. 11(d)) induces a magnetic moment of $0.71 \mu_B$ per unit cell, while the other two adsorption modes bring no influence on magnetism.

3.3.3 Magnetism mechanism analyses

In brief, the variation in magnetism could be understood from L-cysteine adsorption induced distribution of the increasing 3d electron and TM-C interactions: (i) non-bonding 3d electrons for l-cys/MG ($M = \text{V, Cr, Mn}$) adsystems; and (ii) TM-C interactions, influenced by more 3d electrons and the vacancy, for l-cys/MG ($M = \text{Co, Ni, Cu and Zn}$) adsystems.

It is instructive to start the analysis with the VSV complex. The V atom has five valence electrons. One can assume that

RSC Advances

three of them go into the V-C covalent bonds, and one goes into the V-l-cys covalent bond, depicted with double dots in Fig. 12(a), while the fifth (depicted as the circle) replaces the electron of the missing carbon atom. This yields four σ bonds and one π (slightly out-of-plane) bond. Five valences are saturated and the spin is zero, and the binding is strong. In this case, the E_b is the largest among all TM atoms. Cr and Mn have 1 and 2 extra electrons, respectively, which go to separate nonbonding orbitals [red arrows in Fig. 12(a)] and give rise to ~ 1 and $\sim 2 \mu_B$, in agreement with the simple counting rules. With respect to ScSV and TiSV, exhibiting full occupation of bonding orbitals, no change in magnetism happens.

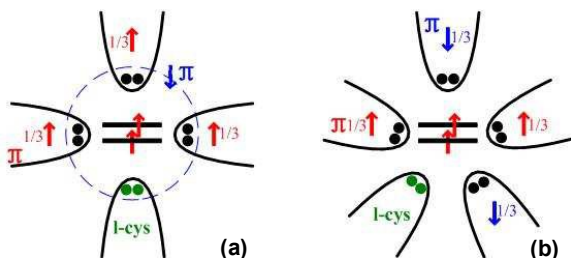


Fig. 12 Schematic representations of the electronic structure of l-cys/MnSV (a) and l-cys/MnDV (b) complexes. Here the numbers “1/3” symbolically represent ligand contribution to the approximate π bond, since one π electron is shared among three π bonds.

For CoSV, NiSV, CuSV and ZnSV adsystems, the TM atom has more than 5 electrons so that some of the nonbonding orbitals are filled. The Coulomb interaction gives rise to a shift of the impurity states into the conduction band, where TM-C hybridization, with large component of graphenic carbon atoms. For l-cys/CoSV and l-cys/CuSV, non-bonding 3d orbitals and TM-C hybridization levels are filled, in agreement with even electron. For l-cys/NiSV and l-cys/ZnSV, the structural strain induced by covalent bonding of l-cys influence TM-C hybridization, induce levels splitting and switch on of magnetism. This is similar to curvature induced magnetism on Ni doped carbon nanomaterials [54, 55] and other kinds of metal doped graphenes [56]. As far as we know, easy determination and control of the local curvature at the location of the dopant Ni in experiments remains a challenge. Herein, our interesting finding demonstrates that controlling cys adsorption on NiSV or ZnSV through different end groups could effectively tune the magnetism and magnetization distribution of the systems, presenting a facile and easy method in experiments. Fe and Zn doped single-vacancy graphenes could also work in specific end-type magnetic applications.

For MDV adsystems, there are five local σ bonds (Fig. 12(b)). The π TM-C interaction is weaker, due to a larger separation between TM and carbon atoms. The π electrons on the dangling bond atoms have opposite spins, deduced by the naked DV graphene, as they are on different sublattices. In this case, V is still the strongest bonding. L-cys/CrDV and l-cys/MnDV show 3d magnetism of 1 and $2 \mu_B$, attributed to 1 and 2 extra electrons. For l-cys/CoDV, initial 3d magnetism of CoDV disappears by formation of a covalent bond with l-cys.

For NiDV, CuDV and ZnDV, weak TM-C interactions induce weak chemisorptions and physisorptions towards l-cys. Only physisorption systems of N-CuDV and N-ZnDV show retention of l-cys radicals magnetism.

With respect to FeG systems, the magnetism sensitively depends on the complicated competition between intra-atomic interactions (Coulomb repulsion and exchange within the 3d levels) and TM-C hybridization. The magnetism could be switched on owing to sensitive disturbances in O-FeSV. Other l-cys/FeSV and l-cys/FeDV systems are non-magnetic.

3.3.4 Magnetization symmetry of MG in l-cys/MG adducts

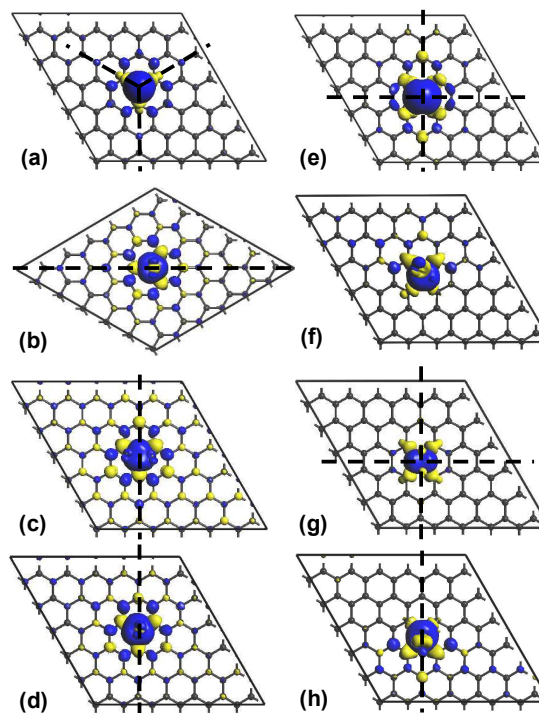


Fig. 13 Schematic top views of spin density distribution on MG in MnSV (a), S-MnSV (b), O-MnSV (c), N-MnSV (d) and MnDV (e), S-MnDV (f), O-MnDV (g), N-MnDV (h). The isovalue is $0.01 e \text{ \AA}^3$. The l-cys atoms in (b-d) and (f-h) were removed to illustrate spin density distribution on the MG surface. The light yellow and dark blue surfaces correspond to majority and minority spins, respectively. The dashed line indicates the mirror line.

Regular magnetization pattern on a substrate could provide a good way to design a substrate with a predefined or controlled magnetization, or provide a substrate with appropriate active sites of catalysis. Regarding spin density distributions on magnetic MSV ($M=V, Cr, Mn, Fe, Co$ and Cu), they show a kind of C_{3v} symmetry (Fig. 13(a)). As for spin density distributions on magnetic MDV ($M=V, Cr, Mn$ and Co), they initially show C_{2v} symmetry (Fig. 13(e)). The C_{2v} symmetry contains two mirror planes. One mirror plane is across the respective geometrical centres of the two 5-member rings and the metal dopant. The other mirror plane is across the

respective geometrical centres of the two 7-member rings and the metal dopant.

The spin density distribution on MSVs exhibits interesting patterns under different adsorption configurations (Fig. 13(b-d) and Fig. S6-S8, ESI†). The spin polarization distributions on CrSV in the O-CrSV adduct, MnSV in the O-MnSV and N-MnSV adducts, FeSV in the O-FeSV adduct and NiSV in the O-NiSV and N-NiSV adducts show the same mirror symmetry. The mirror plane is along one armchair chain containing the metal dopant, which is perpendicular to one lattice vector (Fig. 13(c, d)). In the N-CrSV, S-MnSV, S-NiSV, N-ZnSV adducts, the spin polarization on CrSV, MnSV, NiSV and ZnSV shows mirror symmetry as well. However, this mirror plane is along the longest armchair chain containing the metal dopant in the unit cell (Fig. 13(b)). Magnetization of CrSV in the S-CrSV adduct is nearly symmetric (Fig. S7(b), ESI†). It is noted that we have unveiled switching on of magnetism and magnetization symmetry in l-cys/NiSV adducts in our previous work [45], where Ni was initially doped inside the plane of graphene. The same phenomena found here further demonstrate the stability of such magnetization and magnetization symmetry.

Subsequently we go to magnetism symmetry of the l-cys/MnDV and l-cys/CrDV systems, presenting chemisorption and showing strong magnetism. Only the O-MnDV and O-CrDV adducts retain the initial C_{2v} symmetry, accompanied with two mirror planes (Fig. 13(g) and Fig. S7(g) of ESI†). For the N-MnDV adduct, the mirror plane is across the respective geometrical centres of the two 7-member rings and the metal dopant (Fig. 13(h)). Magnetization of the doped graphene sheet in the S-CrDV and N-CrDV adducts are almost symmetric (Fig. S7(f, h), ESI†). The S-MnDV adduct shows no symmetry of magnetization (Fig. 13(f)). Spin values by the Mulliken spin population method are illustrated in Fig. S8 of ESI† for MnG in l-cys/MnG adsystems.

4. Conclusions

To advance application potentials of TM doped graphene in growing bionanotechnology, our study investigates influences of the TM type and the vacancy type on the interactions between l-cys and TM doped graphenes, including TM (Sc - Zn) doped single-vacancy and double-vacancy graphenes, using the DFT-D approach. This work could provide atomic-scale insights into applications of TM doped graphenes in biosensing, biomolecules immobilization, magnetic bio-separation and other bionanotechnological fields. The main conclusions are summarized as follows.

- (i) TM doping atoms could significantly change chemical reactivity of graphene and lead to strong physical or chemical interactions towards l-cys. Meanwhile, site-specific adsorption towards l-cys is exhibited.
- (ii) The binding energies for l-cys adsorption on MSVs show no obvious variation tendency, while a decreasing tendency from V to Zn emerges for adsorption on MDVs, with emergence of physisorption for the Ni, Cu and Zn doped double-

vacancy graphenes. Starting from Mn to Zn, l-cys adsorption on MDVs is weaker than corresponding adsorption on MSVs. Adsorption mechanism could be understood through combined analyses of the metal dopants and the vacancy types.

- (iii) The l-cys/MG adducts show interesting magnetic properties after l-cys chemisorption. Weakened spin polarization appears on CrG, MnG and CoDV. NiSV could be tuned to be magnetic regardless of the end sites, while FeSV and ZnSV could be tuned to be magnetic selectively by the O-end and the N-end adduction, respectively. The magnetism is influenced by distribution of the increasing 3d electron and TM-C interactions after l-cys adsorption. Most of the magnetization of the chemisorbed systems shows mirror symmetry.

On the basis of the aforementioned conclusions, specific applications of TM doped graphenes could be expected. Cu, Ni and Zn doped double-vacancy graphenes may act as a good sensor platform for L-cysteine. MSVs (M=Sc-Zn) and MDVs (M=Sc-Co) could act as a good immobilization platform toward L-cysteine. Through tuning the transition metal dopant and the vacancy type in doped graphene, site-specific immobilization could be realized. In addition, when magnetic bio-separation or delivery is required, Mn, Cr doped graphenes and Ni doped single-vacancy graphenes could make a facile choice. Fe and Zn doped single-vacancy graphenes could work in specific end-type magnetic applications.

Acknowledgements

This work has been supported by the National Natural Science Foundation of China (Grant No. 51432008, U1435202, 51572223), the “111” Project (Grant No. B08040), the Doctorate Foundation of Northwestern Polytechnical University (Grant No. CX201431). The Centre for High Performance Computing of Northwestern Polytechnical University in Xi'an, China, where the computational work was carried out, is gratefully acknowledged.

References

- 1 M. S. Artiles, C. S. Rout and T. S. Fisher, *Adv. Drug Deliver. Rev.*, 2011, **63**, 1352-1360.
- 2 G. Yang, C. Zhu, D. Du, J. Zhu and Y. Lin, *Nanoscale*, 2015, **7**, 14217-14231.
- 3 K. Yang, L. Feng, X. Shi and Z. Liu, *Chem. Soc. Rev.*, 2013, **42**, 530-547.
- 4 M. Nurunnabi, K. Parvez, M. Nfiujjaman, V. Revuri, H. A. Khan, X. Feng and Y. Lee, *RSC Adv.*, 2015, **5**, 42141-42161.
- 5 L. Tang, Y. Wang and J. Li, *Chem. Soc. Rev.*, 2015, **44**, 6954-6980.
- 6 A. Karimi, A. Othman, A. Uzunoglu, L. Stanciu and S.

RSC Advances

- Andreescu, *Nanoscale*, 2015, **7**, 6909-6923.
- 7 E. Lam and J. H. T. Luong, *ACS Catal.*, 2014, **4**, 3393-3410.
- 8 W. Hu, C. Peng, W. Luo, M. Lv, X. Li, D. Li, Q. Huang and C. Fan, *ACS Nano*, 2010, **4**, 4317-4323.
- 9 Y. Tu, M. Lv, P. Xiu, T. Huynh, M. Zhang, M. Castelli, Z. Liu, Q. Huang, C. Fan, H. Fang and R. Zhou, *Nat. Nanotechnol.*, 2013, **8**, 594-601.
- 10 Z. Kong, W. Zheng, Q. Wang, F. Xi, L. Liang and J.-W. Shen, *J. Mater. Chem. B*, 2015, **3**, 4814-4820.
- 11 W. Qin, X. Li, W.-W. Bian, X.-J. Fan and J.-Y. Qi, *Biomaterials*, 2010, **31**, 1007-1016.
- 12 J. Guo, X. Yao, L. Ning, Q. Wang and H. Liu, *RSC Adv.*, 2014, **4**, 9953-9962.
- 13 H. Vovusha and B. Sanyal, *RSC Adv.*, 2015, **5**, 67427-67434.
- 14 J. Katoch, S. N. Kim, Z. F. Kuang, B. L. Farmer, R. R. Nalk, S. A. Tatulian and M. Ishigami, *Nano Lett.*, 2012, **12**, 2342-2346.
- 15 H. Sun, A. Zhao, N. Gao, K. Li, J. Ren and X. Qu, *Angew. Chem. Int. Edit.*, 2015, **54**, 7176-7180.
- 16 H. Vovusha, S. Sanyal and B. Sanyal, *J. Phys. Chem. Lett.*, 2013, **4**, 3710-3718.
- 17 H. Lei, L. Mi, X. Zhou, J. Chen, J. Hu, S. Guo and Y. Zhang, *Nanoscale*, 2011, **3**, 3888-3892.
- 18 L. Sun, N. Hu, J. Peng, L. Y. Chen and J. Weng, *Adv. Funct. Mater.*, 2014, **24**, 6905-6913.
- 19 S. K. Mudedla, K. Balamurugan and V. Subramanian, *J. Phys. Chem. C*, 2014, **118**, 16165-16174.
- 20 J. Ortiz-Medina, F. Lopez-Urias, H. Terrones, F. J. Rodriguez-Macias, M. Endo and M. Terrones, *J. Phys. Chem. C*, 2015, **119**, 13972-13978.
- 21 J. Guo, T. Zhang, C. Hu and L. Fu, *Nanoscale*, 2015, **7**, 1290-1295.
- 22 Y. Tian, Y. Liu, W. Wang, X. Zhang and W. Peng, *Electrochim. Acta*, 2015, **156**, 244-251.
- 23 M. Li, C. Liu, H. Zhao, H. An, H. Cao, Y. Zhang and Z. Fan, *Carbon*, 2015, **86**, 197-206.
- 24 J. Lu, D. Cui, H. Li, Y. Zhang and S. Liu, *Electrochim. Acta*, 2015, **165**, 36-44.
- 25 S. Liu, J. Zhang, W. Tu, J. Bao and Z. Dai, *Nanoscale*, 2014, **6**, 2419-2425.
- 26 R. Aswathi, M. M. Ali, A. Shukla, K. Y. Sandhya, *RSC Adv.*, 2015, **5**, 32027-32033.
- 27 W. Xiao, R. Zeng, L. Cheng, J. W. Wang, L. J. Jiang and L. G. Wang, *RSC Adv.*, 2015, **5**, 61861-61867.
- 28 K. S. Novoselov, A. K. Geim, S. V. Morozov, D. Jiang, Y. Zhang, S. V. Dubonos, I. V. Grigorieva and A. A. Firsov, *Science*, 2004, **306**, 666-669.
- 29 D. C. Marcano, D. V. Kosynkin, J. M. Berlin, A. Sinitkii, Z. Sun, A. Slesarev, L. B. Alemany, W. Lu and J. M. Tour, *ACS Nano*, 2010, **4**, 4806-4814.
- 30 L. S. Panchokarla, K. S. Subrahmanyam, S. K. Saha, A. Govindaraj, H. R. Krishnamurthy, U. V. Waghmare and C. N. R. Rao, *Adv. Mater.*, 2009, **21**, 4726-4730.
- 31 H. L. Poh, P. Simek, Z. Sofer and M. Pumera, *ACS NANO*, 2013, **7**, 5262-5272.
- 32 M. Khan, M. N. Tahir, S. F. Adil, H. U. Khan, M. R. H. Siddiqui, A. A. Al-warthan and W. Tremel, *J. Mater. Chem. B*, 2015, **3**, 18753-18808.
- 33 A. W. Robertson, B. Montanari, K. He, J. Kim, C. S. Allen, Y. A. Wu, J. Olivier, J. Neethling, N. Harrison, A. I. Kirkland and J. H. Warner, *Nano Lett.*, 2013, **13**, 1468-1475.
- 34 H. Wang, Q. Wang, Y. Cheng, K. Li, Y. Yao, Q. Zhang, C. Dong, P. Wang, U. Schwingensschlögl, W. Yang and X. X. Zhang, *Nano Lett.*, 2012, **12**, 141-144.
- 35 A. V. Krashennnikov, P. O. Lehtinen, A. S. Foster, P. Pyykkö and R.M. Nieminen, *Phys. Rev. Lett.*, 2009, **102**, 126807.
- 36 L. Tsetseris, B. Wang and S. T. Pantelides, *Phys. Rev. B*, 2014, **89**, 035411.
- 37 C. B. Crook, C. Constantin, T. Ahmed, J.-X. Zhu, A. V. Balatsky and J. T. Haraldsen, *Sci. Rep.*, 2015, **5**, 12322.
- 38 H.-X. Luan, C.-W. Zhang, S.-S. Li, R.-W. Zhang and P.-J. Wang, *RSC Adv.*, 2013, **3**, 26261-26265.
- 39 E. J. G. Santos, A. Ayuela and D. Sánchez-Portal, *New J. Phys.*, 2010, **12**, 053012.
- 40 H. Zhang, X. Luo, X. Lin, X. Lu and Y. Leng, *Int. J. Hydrogen Energ.*, 2013, **38**, 14269-14275.
- 41 Z. Teng, Q. Xue, M. Shan, Z. Jiao, X. Zhou, C. Ling and Z. Yan, *J. Phys. Chem. C*, 2012, **116**, 19918-19924.
- 42 S. A. Tawfik, X. Y. Cui, S. P. Ringer and C. Stampfl, *RSC Adv.*, 2015, **5**, 50975-50982.
- 43 E. H. Song, J. M. Yan, J. S. Lian and Q. Jiang, *J. Phys. Chem. C*, 2012, **116**, 20342-20348.
- 44 S. Impeng, P. Khongpracha, J. Sirijaraensre, B. Jansang, M. Ehara and J. Limtrakul, *RSC Adv.*, 2015, **5**, 97918-97927.
- 45 H. Luo, H. Li, Q. Fu, Y. Chu, X. Cao, C. Sun, X. Yuan and L. Liu, *Nanotechnology*, 2013, **24**, 495702.
- 46 A.-C. Liu, D. Chen, C.-C. Lin, H.-H. Chou and C. Chen, *Anal.*

- Chem.*, 1999, **71**, 1549-1552.
- 47 A. Kühnle, T. R. Lindroth, M. chunack and F. Besenbacher, *Langmuir*, 2006, **22**, 2156-2160.
- 48 B. Delley, *J. Chem. Phys.*, 2000, **113**, 7756-7764.
- 49 S. Grimme, *J. Comput. Chem.*, 2006, **27**, 1787-1799.
- 50 J. L. Fajin, J. R. Gomes and M. N. Cordeiro, *Langmuir*, 2013, **29**, 8856-8864.
- 51 B. Höfiling, F. Ortmann, K. Hannewald and F. Bechstedt, *Phys. Rev. B*, 2010, **81**, 045407.
- 52 B. Cordero, V. Gómez, A. E. Platero-Prats, M. Revés, J. Echeverria, E. Cremades, F. Barragán and S. Alvarez, *Dalton Trans.*, 2008, **21**, 2832-2838.
- 53 L. Zhang and Z. Xia, *J. Phys. Chem. C*, 2011, **115**, 11170-11176.
- 54 E. J. G. Santos, A. Ayuela and D. Sánchez-Portal, *J. Phys. Chem. C*, 2012, **116**, 1174-1178.
- 55 Y.-L. Mao, X.-H. Y. and Y. Xiao, *Nanotechnology*, 2005, **16**, 3092-3096.
- 56 B. Huang, J. Yu and S.-H. Wei, *Phys. Rev. B*, 2011, **84**, 075415.

Graphical Abstract

Unprotonated L-cysteine is docked on single-vacancy and double-vacancy graphenes doped with the transition metal from Sc to Zn. The adsystems exhibit interesting adsorption stability and magnetism.

